Revista Mexicana de Astronomía y Astrofísica, **50**, 323–328 (2014)

KINEMATICS OF THE GALACTIC SUPERNOVA REMNANT G206.9+2.3

P. Ambrocio-Cruz,[1] M. Rosado,[2] E. Le Coarer,[3] A. Bernal,[2] and L. Gutiérrez[4]

Received February 17 2014; accepted August 1 2014

RESUMEN

Se realizó un estudio cinemático del remanente de supernova galáctico G206.9+2.3 (PKS 0646+06) en las líneas [SII]λ6717 y 6731 Å. Este es uno de los primeros pasos de un proyecto a largo plazo de determinación de distancias cinemáticas a RSN galácticos con contraparte óptica. Se obtuvo la distancia cinemática a esta nebulosa, mostrando primero que los filamentos detectados son realmente la contraparte óptica del RSN en radio. La distancia estimada en este trabajo es ligeramente mayor que la distancia de Monoceros. Se estimó que G206.9+2.3 está localizada a 2.2 kpc del Sol, en una región del cielo donde se observan varias nebulosas superpuestas a diferentes velocidades. Se midió una velocidad de choque de 86 km s^{-1} y un diámetro lineal de 18 pc. Finalmente se calculó que la energía depositada al medio interestelar por la explosión de supernova es de 1.7×10^{49} ergs por lo que se concluyó que G206.9+2.3 está en la fase radiativa de su evolución, con una edad de 6.4×10^4 años.

ABSTRACT

We studied the kinematics of the galactic supernova remnant (SNR) G206.9+2.3 (PKS 0646+06) in the [SII]λ6717 and 6731 Å lines, as one of the initial steps of a long-term project to determine kinematical distances to galactic SNRs with optical counterparts. We obtained the kinematic distance to this nebula by first showing that the filaments detected were in fact the optical counterpart of the radio SNR. The distance estimated here is slightly greater than that of the Monoceros Loop. We estimate that G206.9+2.3 is located about 2.2 kpc from the Sun, in a zone where several background and foreground nebulae at different velocities are seen in projection. We measured a shock velocity of 86 km s^{-1} and a linear diameter of 18 pc. Finally, we calculated the energy deposited in the interstellar medium by the SN explosion as 1.7×10^{49} ergs and concluded that the SNR is in the radiative phase of evolution with an age of 6.4×10^4 years.

Key Words: HII regions — ISM: individual objects (G206.9+2.3) — ISM: kinematics and dynamics — ISM: supernova remnants

1. INTRODUCTION

The study of supernovae (SNe) and their remnants has occupied a central role in astrophysics; they have a profound effect on the morphology, kinematics, and ionization balance of galaxies, and they possibly trigger generations of new stars. SN explosions are one of the most violent events in the universe, as they can release energies of the order 10^{49} to 10^{51} erg as well as inject heavy elements into the interstellar medium (ISM) and hundreds of neutrinos. The shock wave and the ejected material expand into the surrounding ISM, sweeping up gas and dust and creating a shell. This shell of ejected and swept-up material is known as a supernova remnant (SNR). The ejected material forms a shock wave, causing a rise in ambient temperatures and releasing relativistic particles that produce non-thermal emissions. Essentially, accelerated electrons spiraling in their associated magnetic fields produce synchrotron radiation from the SNRs, which that makes them easily detectable as radio sources with non-thermal spectral indices. SNRs are also often seen in X-rays, but with different shapes compared to their radio counterparts, generating both thermal and non-thermal radiation. SNRs are most conveniently studied via their radio signatures due to their strong emission in this part of the electromagnetic spectrum. In our Galaxy, there are about 274 SNRs (Green 2009) catalogued by their radio emission, of which only about 29% have optical counterparts (Green 2009; Stupar &

[1]Instituto de Ciencias Básicas e Ingeniería, Universidad Autónoma del Estado de Hidalgo, Mexico.
[2]Instituto de Astronomía, Universidad Nacional Autónoma de México, Mexico.
[3]Laboratoire d'Astrophysique de Grenoble, Université Joseph Fourier, France.
[4]Instituto de Astronomía, Universidad Nacional Autónoma de México, Ensenada B.C., Mexico.

Parker 2011). Much research has been performed on this subset of objects because optical data complement studies at other wavelengths and allow us to determine the physical and chemical conditions of the SNRs as well as their distances, because of the existence of optical emission lines, such as Hα or [SII]6717 Å that allow us to measure the Doppler shift of the lines; however, optical kinematic data are scarce. We have started a survey of Galactic SNRs in the northern hemisphere of the Galaxy with optical counterparts by means of a scanning Fabry-Perot (FP) interferometer surveying the [SII](6717 and 6731 Å) and Hα lines. This provides us a homogeneous set of data from SNRs as well as from their environment. These data are important for the accurate determination of kinematic distances to these objects. Indeed, one of the aims of this project is to establish reliable kinematic distances for SNRs, and this determination will require a large sample of data.

The present work is another step of the aforementioned project, the first of which involved studying three southern SNRs (Rosado et al. 1996). The present work studies the kinematics of SNR G206.9+2.3 in [SII] lines, with the principal aim of determining its kinematic distance. In addition, our kinematic data allow us to derive the shell expansion velocity, the initial energy of the SN explosion, the evolutionary stage, and the SNR age. In § 2, we describe our observations and data reduction. The properties and local environment of the SNR G206.9+2.3 as well as the kinematic properties resulting from the present work will be presented in § 3. Finally, a discussion and summary of our data and results are presented in § 4.

2. OBSERVATIONS AND DATA REDUCTION

Observations were carried out on December 10, 2012 with the UNAM Scanning Fabry-Pérot interferometer, PUMA (Rosado et al. 1995), which was attached to the f/7.9 Ritchey-Chretien focus of the 2.1 m telescope of the Observatorio Astronómico Nacional at San Pedro Mártir, B.C., México. The PUMA instrument uses a Marconi2 2048×2048 pixel CCD detector with a pixel size of 13.5 μm. A 512×512 pixel window was used, and a 4×4 binning was performed, giving a pixel equivalent to 2.34 arcsec on the sky. Table 1 reports the main characteristics of the instrumental setup and presents the journal of observations.

We obtained direct images in the lines Hα and [SII]λ6717 and 6731 Å using the PUMA in direct image mode. The exposure time of each of the direct images was 120 s. The CCD reading was binned 4×4, giving a pixel size of 2.34 arcsec and a field of view of 10′. In addition, we obtained scanning FP interferometric data cubes in the [SII]λ6717 and 6731 Å lines. The [SII] cubes share the same scale and field of view as the direct images. The phase calibration was made by taking data cubes of a calibration neon lamp after the SNR exposure. The FP data cube was composed of 48 steps, with integration times of 120s per step, giving a total exposure time of 1.6 hours. In this form, the final data cube dimensions were $512 \times 512 \times 48$.

TABLE 1

JOURNAL OF OBSERVATIONS AND PARAMETERS OF THE FP INTERFEROMETRIC OBSERVATION

Observation Telescope	OAN-SPM 2.1m
Date	2012 December 10
Detector	Marconi2 CCD
Instrument	PUMA
FP scanning steps	48
Finesse	24
Filter	[SII]
Central wavelength (Å)	6720
FWHM (Å)	20
Interference order	322
Free spectral range ($\mathrm{km\,s^{-1}}$)	930
Sampling resolution ($\mathrm{km\,s^{-1}}$/channel)	19.4
Calibration line	6717.04 Ne
Binning	4×4
Final pixel size (arcsec)	2.34

The two [SII]λ6717 and 6731 Å lines that we observed fall in the free spectral range, separated by 291 $\mathrm{km\,s^{-1}}$, with the λ6731 Å line being less intense; this means that we are at the low density limits.

Data reduction was carried out using the software package CIGALE (Le Coarer et al. 1993). Our data cube is not contaminated by sky line emission. To extract kinematic information from the FP data cube, we divided the filament into several small boxes over which we obtained several radial velocity profiles in order to seek an expansion motion revealed by line splitting of the velocity profiles.

The radial velocity profiles were fitted by Gaussian functions after deconvolution by the instrumental function (an Airy function). In this way, we obtained the radial velocity of one or several components in the region of interest. The computed widths of the Gaussian functions give the velocity dispersion, σ_v, of the velocity component, corrected for the instrumental response function. The CIGALE software enabled us to separate the monochromatic emissions from the continuum.

3. THE SNR G206.9+2.3

The constellation of Monoceros is remarkably rich in extended Galactic radio sources. Large parts of this constellation over a wide range have been mapped in the radio continuum, and mapping has also been done in the optical. These observations have revealed a com-

plicated location with a mixture of thermal and nonthermal emissions, and this confirms the complexity of the region containing the large HII region NGC 2237-46 (Rosette Nebula). The SNR G206.9+2.3 (also known as PKS 0646+06) is located at the eastern edge of the Monoceros Ring Nebula and was first noted by Holden (1968) at 178 MHz.

Caswell (1970), Haslam & Salter (1971), and Graham et al. (1982) demonstrated that G206.9+2.3 possessed a nonthermal radio continuum spectrum, which was recently confirmed by Gao et al. (2011). On morphological grounds, Haslam & Salter (1971) concluded that the radio source probably represents a SNR in its own right rather than a component of the nearby Monoceros SNR. Optical filaments coinciding with the radio source were noted by both Davies and Meaburn (1978) and by van den Bergh (1978). The detailed optical photograph by Davies and Meaburn in the Hα+[NII] wavelength shows an ellipse of fine filaments, containing some internal filamentary structure. Rosado (1982) from Hα, [SII] and [OIII] plates deduced that the optical emission, detected at the same location of the nonthermal radio source, is characteristic of a SNR, given their high [SII]/Hα line ratio. Einstein IPC imaging observations east of the Monoceros supernova remnant revealed a region of enhanced X-ray emission. Leahy (1986) identified this X-ray emission with the SNR G206.9+2.3. The radio contours from Graham et al. (1982) cover a significantly larger area than the map of Day et al. (1972). It should be noted, however, that neither the optical emission (Davies and Meaburn, 1978) nor the X-ray emission (Figure 1 in Leahy 1986) fill the radio emission region.

The distance to G206.9+2.3 was estimated to be from about 3 kpc to 5 kpc by Graham et al. (1982), through radio observations and by employing the surface brightness-linear diameter ($\Sigma - D$) relationship. Rosado (1982) noted that [OIII] emission from SNRs comes from shocks faster than 60 km s^{-1}, and that the computed upper limit to the distance of this SNR can be obtained by taking the two values for E_0/n_0 of 10^{50} and 10^{51}, and thus a distance range from 3 to 6.5 kpc is derived. Leahy (1986), from the X-ray emission of the SNR PKS 0646+06 (Einstein observations) derived a distance between 3 and 11 kpc; the author also derived its age as 60,000 years from the observed X-ray flux and temperature, using a Sedov model.

At the top of Figure 1 we show the Hα image of the SNR G206.9+2.3 taken from Davies and Meaburn (1978). The position of the filaments studied in this work is indicated by squares. Towards the bottom of Figure 1, we show the Hα and [SII]λ6717 Å + λ6731 Å of the central (left) and southern (right) filaments obtained from our observations, discussed in § 2.

To obtain information on the kinematics of the filaments we integrated the emission over the whole of each individual filament. The extracted velocity profiles were analyzed by fitting one or more Gaussians once deconvolution with the FP instrumental function was achieved. Figure 2 shows the radial velocity profiles of each filaments; a bright component at $V_{\rm LSR} \approx 22 \pm 5$ km s^{-1} is common to both filaments. This component is broad and the width varies between 39 km s^{-1} and 58 km s^{-1}. In addition to this bright component, the southern filament profile shows another two components at $+398 \pm 5$ km s^{-1}, with a width of 97 km s^{-1}, and at -269 ± 5 km s^{-1}, with a width of

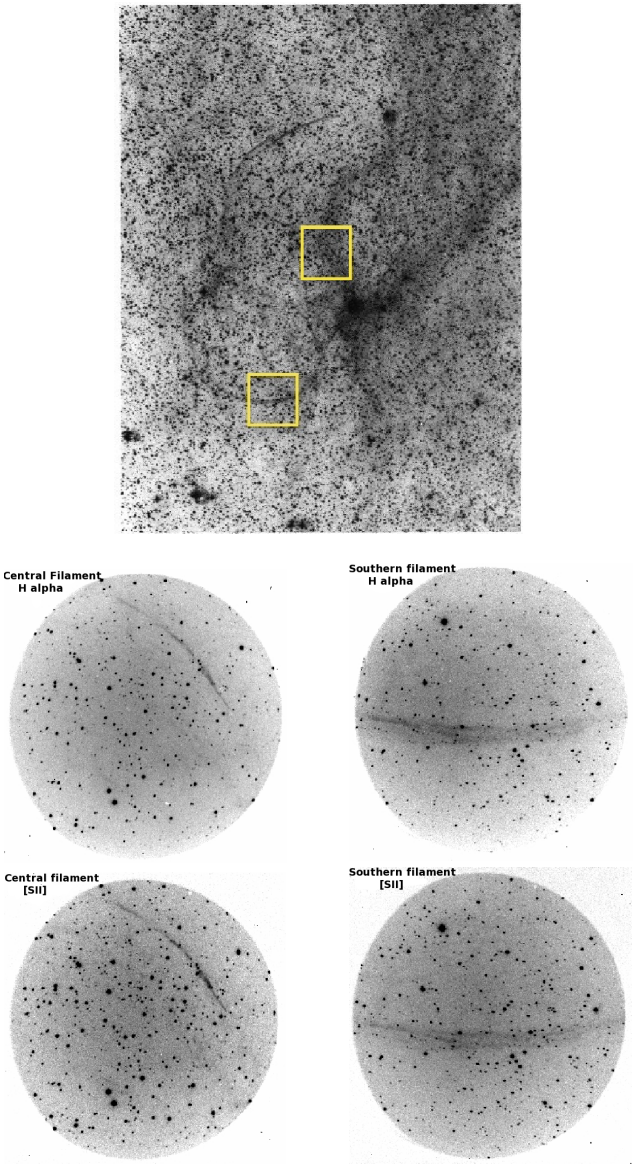

Fig. 1. Top: the Hα image of the SNR G206.9+2.3 taken from Davies & Meaburn (1978). The position of the filaments studied in this work is indicated by squares. Bottom: the Hα and [SII]6717 Å images of the central (left) and southern (right) filaments obtained from our observations; the field of view is 10′. North is at the top and east is at the left for all images.

TABLE 2

KINEMATIC PARAMETERS OF THE SNR G206.9+2.3

V_{sys} km s^{-1}	V_{exp} km s^{-1}	d kpc	l^{II} °	R pc
22 km s^{-1}	86 km s^{-1}	2.2	206.9	18

NOTES: V_{sys}: Systemic velocity of the region referred to the LSR; d: distance to the SNR; R: Linear radius of the SNR calculated from the radio angular diameter (57′).

TABLE 3

MAIN PARAMETERS OF THE SNR G206.9+2.3 DERIVED IN THIS WORK

Linear radius	18pc
Shock velocity	86 km s^{-1}
Energy deposited in the ISM by the SN explosion	1.7×10^{49} ergs
Age	6.4×10^4 yr
Phase	Radiative

58 km s^{-1}. Moreover, the central filament presents a more complex profile, showing several components at -64 ± 5 km s^{-1}, -267 ± 5 km s^{-1}, -349 ± 5 km s^{-1} and $+388 \pm 5$ km s^{-1} (in order of intensity) with widths of 49 km s^{-1}.

All filaments we see are mostly moving sideways, because these are typically highly compressed and, therefore, very thin. Only when they move sideways can we look along them and have a long line of sight through them; only then can we distinguish their emission easily from the background. Filaments moving towards us or away from us should be very smooth and faint, simply because our line of sight through them is very short and they should extend and project to the plane of the sky. Therefore, we may not be able to distinguish them easily from the background. The thin filaments that move mostly sideways can be found, in principle, anywhere around the origin of the explosion, because a well-structured environment can slowdown the shock wave in some directions more rapidly than in others. Both the central and southern filaments contain the $+22 \pm 5$ km s^{-1} component. In both cases, it is the brightest component, and the filamentary structures are the brightest features in both images, as well. They also both have a fainter counterpart of the fainter SII line at the appropriate velocity of $\approx -268 \pm 5$ km s^{-1} (the "apparent" negative velocities correspond to a miscalculation of the software, given that it takes the λ6717Å line as the rest λ; see Figure 2 for further details).

If the shell is expanding spherically from the geometrical center, due to projection effects the maximum velocity difference is found at the center of the remnant. Filaments moving towards and away from us should only be visible in the interior of the SNR and not at its edge. To find these filaments, we have to look in the central profile for lines that are not present in the southern profile. Clearly the -64 ± 5 km s^{-1} and -349 ± 5 km s^{-1} pair fits this description. The separation agrees with the distance between the two SII lines and the -64 ± 5 km s^{-1} component is brighter than the other component. In this case, as the component at 22 ± 5 km s^{-1} is detected in both filaments, we consider that this is the systemic velocity of the SNR, and that we are observing only one side of the expansion shell, which is moving at a velocity of -64 ± 5 km s^{-1}. Consequently, the expansion velocity of the SNR is $+86$ km s^{-1}. Since we do not know exactly where the supernova originated, this velocity is only the lower limit to the actual expansion velocity, since it might also have a transverse component, which we cannot determine.

From the study by Brand & Blitz (1993) it is clear that Perseus arm HII regions do not follow purely circular rotation. If G206.9+2.3 is about 2 kpc away, it is likely a Perseus arm object. In Table 2 we have quoted the systemic velocity of the SNR, as well as the derived kinematic distance, assuming that it follows a non-circular rotation law, for which we have used the velocity field derived by Brand & Blitz (1993).

The distance estimated here (2.2 kpc) is slightly greater than that of the Monoceros nebulosity calculated by Graham et al. (1982), of 1.6 kpc, and it is greater that obtained by Lozinskaya (1972), of 1 kpc.

The uncertainty of the systemic velocity (± 5 km s^{-1}) of the SNR and the uncertainty associated whith the velocity dispersion of the gas that has been compressed and illuminated (± 2 km s^{-1}) correspond to an uncertainty of 0.7 kpc in distance. Table 3 provides several parameters of G206.9+2.3 obtained from our distance estimate. The pre-shock density (0.1 cm^{-3}) was taken from Leahy (1986). The value of the age and the initial energy deposited in the ISM by the SN explosion derived here and quoted in Table 3 is typical of a SNR. The energy and age of the SNR were obtained under the assumption that the SNR is in the radiative phase. The uncertainty related to the velocity expansion and the uncertainty of the radius (30%) leads to an uncertainty of 80% in the kinetic energy.

In our observations, we detected the two lines [SII] (λ6717 Å and λ6731 Å). By taking the peak intensity of the two components, a high [SII]λ6717/[SII]λ6731 line ratio of 4.8 was obtained, placing the SNR at the low density limit.

In an attempt to explain the other component at $+398 \pm 5$ km s^{-1}, we hypothesize that we are observing another shocked region towards the south of

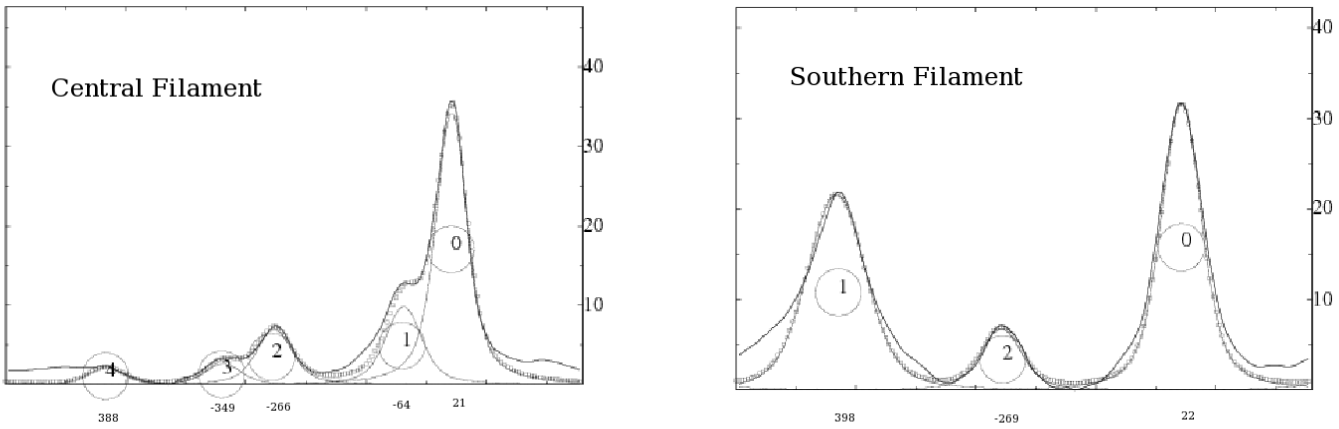

Fig. 2. Radial velocity profiles for each of the filaments. The central filament profile is displayed on the left and the southern filament profile on the right. The X axes are the LSR velocities in km s^{-1} and the Y axes are the intensity of the line in arbitrary units. (0) and (2) profiles correspond to [SII]λ6717 and [SII]λ6731 lines respectively (this latter line gives false negative velocities) separated by 291 km s^{-1}. We can observe that the two lines of [SII] have different intensity, placing the SNR at the low density limit.

G206.9+2.3, but more distant; we have calculated a distance for this shocked region of 6 kpc. This shocked region has a velocity dispersion of 97 km s^{-1}. Moreover, this velocity component is mainly detected at the center of the southern filament.

It should be noted that the whole images were averaged to construct the radial velocity profiles.

4. SUMMARY

In this work we studied the kinematics of the galactic SNR G206.9+2.3, and subsequently obtained its kinematic distance. The distance estimated here is slightly greater than that of the Monoceros Loop. The kinematic distance obtained from this work is also smaller that those determined by radio and X-ray, ranging from 3 kpc to 11 kpc. The value of the initial energy deposited in the ISM by the SN explosion and the age of the SNR derived here and quoted in Table 3 are typical of SNRs in the radiative phase. Furthermore, the profiles allowed us to determine the velocity of the shock in the optical filaments as reported in Table 3. The supernova remnant G 206.9+2.3, displays a good agreement between the optical and radio structures, and its probable distance from the Sun calculated in this work suggests an association with the Perseus spiral arm.

Moreover, we have detected another shocked region toward the south of G206.9+2.3, but 4 kpc farther than the SNR.

We wish to thank the referee for carefully reading the manuscript and for providing valuable comments and suggestions, which have helped us improve the manuscript. This work was partially financed by PROMEP- Incorporación de Nuevos PTC (UAEH-PTC-514).

REFERENCES

Brand, J., & Blitz, L. 1993, A& A, 275, 67
Caswell, J. L. 1970, Australian J. Phys., 23, 105
Davies, R. D., & Meaburn, J. 1978, A& A, 69, 443
Day, G., Caswell, J., & Cooke, D. 1972, Australian J. Phys. Astrophys. Supp., 25, 1
Gao, X. Y., Han, J. L., Reich, W., Reich, P., Sun, X. H. & Xiao L. 2011, A& A, 529, 159
Graham, D. A., Haslam, C. G. T., Salter C. J. & Wilson W.E. 1982, A& A, 109, 145
Green, D.A. 2009, A Catalogue of Galactic Supernova Remnants, available online at `http://www.mrao.cam.ac.uk/surveys/snrs/`
Haslam, C. G. T., & Salter, C. J. 1971, MNRAS, 151, 385
Holden, D. J. 1968, MNRAS, 141, 57
Leahy, D. A. 1986, A&A, 156, 191
Le Coarer, E., Rosado, M., Georgelin, Y., et al. 1993, A&A, 280, 365
Lozinskaya, T. A. 1972, Soviet Astron., 15, 910
Rosado, M. 1982, ReMexAA, 5, 127
Rosado, M., Langarica, R., Bernal, A. et al. 1995, ReMexAA(SC), 3,268
Rosado, M., Ambrocio-Cruz, P., LeCoarer, E., & Marcelin, M. 1996, A&A, 315, 243
Stupar, M., & Parker, Q. A. 2011, MNRAS, 414, 2282
van den Bergh, S. 1978, ApJ, 220, 171

P. Ambrocio-Cruz:Instituto de Ciencias Básicas e Ingeniería, Universidad Autónoma del Estado de Hidalgo, Ciudad Universitaria, Km 4.5 Carretera Pachuca-Tulancingo; Col. Carboneras C.P. 42184, Mineral de la Reforma, Hidalgo, Mexico (patricia@astro.unam.mx).
L. Gutiérrez: Instituto de Astronomía, Universidad Nacional Autónoma de México, Ensenada, B.C., Mexico (leonel@astro.unam.mx).
E. LeCoarer: Laboratoire d'Astrophysique de Grenoble, Université Joseph Fourier, B.P. 53 Grenoble CEDEX 9, France (Etienne.Le-Coarer@obs.ujf-grenoble.fr).
M. Rosado and A. Bernal: Instituto de Astronomía, Universidad Nacional Autónoma de México, Apdo. Postal 70-264, México, D.F., 04510, Mexico (margarit, abel@astro.unam.mx).